SUPPORTING INFORMATION

Glucose/fructose-based boric acid-bridged in-situ generated macrocyclic polymers and their behaviors in capturing dyes

Zhaona Liu[1,2†], Make Li[2†], Yangyang Zheng[2†], Huacheng Zhang[2*]

[1]Department of Pharmacy, Medical School, Xi'an Peihua University, Xi'an 710125, China

[2]School of Chemical Engineering and Technology, Xi'an Jiaotong University, Xi'an 710049, Shaanxi, China

*Corresponding author. E-mail: zhanghuacheng@xjtu.edu.cn (H. Zhang)

†Three authors contributed equally to this work.

Experimental section about materials and methods

1 Materials

Anhydrous ethanol was purchased from Beijing Macklin Biochemical Company. The G, F (99%), BA (>99.5%), anhydrous ethanol (>99.5%), MB (>98%) and MG (Scheme S1) were all purchased from Macklin (Shanghai, China) without further purification. The RB was purchased from Tianjin Heowns Biochemical Technology Company. Ultrapure water was directly produced in our lab by Ultra-pure water system.

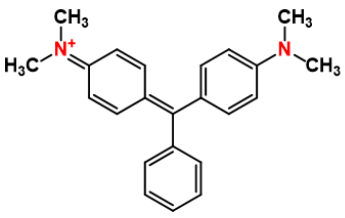

MG

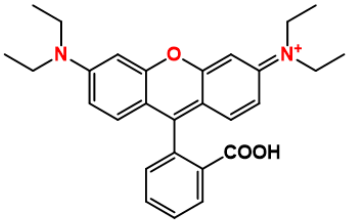

RB

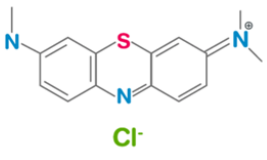

MB

Scheme S1 Chemical structures of dyes employed in this work.

2 Synthesis of BA-G and BA-F

Weigh 5 g of BA and 1 g of G, add them to the beaker, and then heat them to 40 ℃ with 40 mL of water to dissolve them completely. The beaker was sealed with tinfoil and then reacted in a reaction oven at 200 ℃ for 4 h. After the reaction, the beaker was soaked with ultrapure water several times and centrifuged until the supernatant was clear in color. The BA-G polymer was obtained by drying the sample.

Similarly, 2 g of BA and 1 g of F were weighed and added to a beaker, and heated to a certain temperature with 40 mL of water to dissolve them completely. The beaker was sealed with tinfoil and the reaction was carried out in a reaction oven at 220 ℃ for 4 h. After the reaction, the beaker was soaked with ultrapure water several times and centrifuged until the supernatant was clear in color. The BA-F polymer was also obtained after drying the sample.

3 Characterization

The morphology of the BA-G and BA-F was observed by scanning electron microscopy (SEM) (MAIA3 LMH, Warrendale, PA, USA). Energy dispersive X-ray spectrometry (EDS, Aztec X-max N-50 mm^2, Concord, MA, USA) was used to study the elemental distribution in the adsorbent.

The chemical properties of the synthesized materials were analyzed by Fourier transform infrared spectroscopy (FT-IR) (Nicolet iS50) in the range of 4000-400 cm^{-1}. X-ray diffraction (XRD) analysis was carried out by using a Shimadzu XRD-6100 and Cu Kα radiation (conditions: λ = 0.15406 nm, 100 mA, 40 kV, scanning rate 6° min^{-1}) in the range of 2θ = 10°~80°). Thermogravimetric analysis (TGA) and differential thermogravimetric analysis (DTG) were carried out in the range of 30-800 °C by using a Netzsch STA 449 F3 from Germany with a ramp rate of 10 °C min^{-1} to test the stability of the adsorbent under nitrogen gas atmosphere.

The specific surface area of the adsorbent was analyzed by using the N_2 adsorption-desorption method (TriStar II 3020 3.02) through the Brunauer-Emmett-Teller (BET) equation. A certain amount of adsorbent was evacuated

at 120 °C for 8 h before the specific surface area test, and the adsorption and desorption isothermal curves for N_2 were tested using the standard static volume method in a 77 k N_2 cold trap.

X-ray photoelectron spectroscopy (XPS) data were obtained by Thermo Fisher ESCALAB Xi photoelectron (Waltham, MA, USA) by using Al Kα excitation. A UV-vis absorption spectrometer (TU-1901 Beijing Pukinje GENERAL Instrument Co., Ltd., Beijing, China) was used to determine the concentration of residual dyes in the supernatant by measuring the standard curves at the maximum wavelengths of each dye.

4 Adsorption experiment

4.1. Determination of dyes solution standard curve

Standard solutions (2.0, 4.0, 6.0, 8.0, 10.0, 15.0, 20.0 and 25.0 mg L^{-1}) of each dye in the concentration range of 2.0-25.0 mg L^{-1} were prepared. The absorbance of the solutions was measured at the maximum wavelength of the dyes. The concentration of the solution (C, mg L^{-1}) was taken as the horizontal coordinate, and the absorbance (Abs) was taken as the vertical coordinate to fit the standard curves for each dye as shown in Fig. S1.

4.2. Single adsorption performance studies

In a 100 mL conical flask, 30 mL of dye solution was added, then 10 mg of adsorbent was added. Then, the top of the flask was sealed with cling film and placed in a gas bath constant temperature oscillator. It was oscillated at a certain temperature at an oscillation rate of 130 r min^{-1} until the adsorption reached equilibrium. The subsequent experiments were carried out at pH=7. The concentration of the adsorbed dye was determined by using UV-vis spectra, and the remaining concentration of the solution was determined from the standard curve. The adsorption capacity of the adsorbent for the dye, q_e (mg g^{-1}), and the removal rate, R%, were calculated by Eqs. (1) and (2).[1,2]

$$q_e = \frac{(C_0 - C_e)V}{m} \qquad (1)$$

$$R\% = \frac{C_0 - C_e}{C_0} \times 100\% \quad (2)$$

Where C_0 (mg L^{-1}) and C_e (mg L^{-1}) are the concentration of dyes in the beginning and then at equilibrium time, respectively. V (L) and m (g) are the volume of the dyes and the weight of the adsorbent, respectively.

4.3. Single-factor experiments

The effects of the mass ratio of BA to G/F, reaction temperature and reaction time on the adsorption properties of BA-G/F were investigated. The effects of different conditions on the adsorption properties of BA-G were investigated when the mass ratio of BA to G was 5:1, the reaction temperature was 200 ℃, and the reaction time was kept at 4 h. When the mass ratio of BA to F was 2:1, the effects of different mass ratios on the adsorption properties of BA-F were investigated at a reaction temperature of 220 ℃ and a reaction time of 4 h. The results are shown in Fig. S2.

4.4. Recyclability of BA-G and BA-F

Adsorbent performance can usually be evaluated by reusability. Use the previous vibration conditions and stop the adsorption when it has reached equilibrium. After filtering the adsorbent through sand filtration equipment, the adsorbent is washed with an ethanol solution in several soaks, which can wash out the dyes. The adsorbent was then dried to a constant weight and the next repeated adsorption could be continuously performed. The reusability of the adsorbent can be assessed based on the results of the repeated cycles of this experiment.

5 Adsorption kinetics

Adsorption kinetics can demonstrate the adsorption process versus time. We used quasi-first-order kinetic models and quasi-second-order kinetic models to analyze the adsorption of BA-G and BA-F on various types of dyes.[3]

$$\log\left(q_e - q_t\right) = logq_e - \frac{K_1 t}{2.303} \quad (3)$$

$$\frac{t}{q_t} = \frac{1}{K_2 q_e^2} + \frac{t}{q_e} \quad (4)$$

K_1 (min^{-1}) and K_2 (g mg^{-1} min^{-1}) are the adsorption rate constants and pseudo-second-order adsorption rate constants, respectively. The q_e (mg g^{-1}) is the adsorption capacity, and the q_t (mg g^{-1}) is the occasional adsorption capacity.

6 Adsorption isotherm

The equilibrium adsorption results were fitted by using the Langmuir and Freundlich adsorption isotherm model to obtain data related to the maximum adsorption capacity.[4]

$$\frac{C_e}{q_e} = \frac{C_e}{q_m} + \frac{1}{K_L q_m} \quad (5)$$

$$\ln\left(q_e\right) = lnK_F + \frac{1}{n} ln(C_e) \quad (6)$$

C_e (mg L^{-1}) is the equilibrium concentration, q_e (mg g^{-1}) is the equilibrium adsorption capacity, q_m is the maximum adsorption capacity, K_F and n are constants of the Freundlich equation, as well as K_L is constant for the Langmuir equation.

7 Adsorption thermodynamics

Adsorption thermodynamics can determine whether the adsorption process is either exothermic or absorptive. It can also determine whether the adsorption process is spontaneous or not.[5,6]

$$K_d = \frac{q_e}{C_e} \quad (7)$$

$$lnK_d = \frac{\Delta S^0}{R} - \frac{\Delta H^0}{RT} \quad (8)$$

$$\Delta G^0 = \Delta H^0 - T\Delta S^0 \quad (9)$$

K_d (L g^{-1}) is the distribution factor, q_e (mg g^{-1}) is the equilibrium adsorption capacity, C_e (mg L^{-1}) is the equilibrium concentration, R (8.314 J mol^{-1} K^{-1}) is

the general gas constants, as well as T (K) is the absolute temperature.

8 Theoretical calculations

Theoretical calculations of the adsorption system were carried out by using the DFT method, which can accurately analyze the intermolecular interaction energy. The Gaussian quantum chemistry software was used to optimize the geometry of the constructed polymeric model and calculate the binding energy, charge distribution and orbital interactions with the dye molecules, as well as to elucidate the mechanism of the adsorption process at the molecular level.

The solvent effect of water was first described by using the CPCM implicit solvent model, and to find the optimal adsorption structure of polymers with dyes. One hundred possible complex structures were randomly generated, then performed the search by using the Molclus program, and were optimized for each complex cluster by using the xTB program.[7] After preliminary structure optimization, the cluster with the lowest energy was selected as the most probable adsorption structure and then these selected clusters were optimized. All the above calculations were performed by using ORCA 5.02 program.[8] The adsorption energy of the complex was calculated by the following equation:

$$E_{adsorb} = E_{A+B} - E_A - E_B \qquad (10)$$

Where E_A and E_B are the energies of the isolated molecules and E_{A+B} is the total energy of the complex structure.

To further analyze the intermolecular interactions, an independent gradient model (IGM) [9] was carried out by using the Multiwfn program [10] to visually study the weak interactions, and the VMD program [11] was also used to observe the interactions.

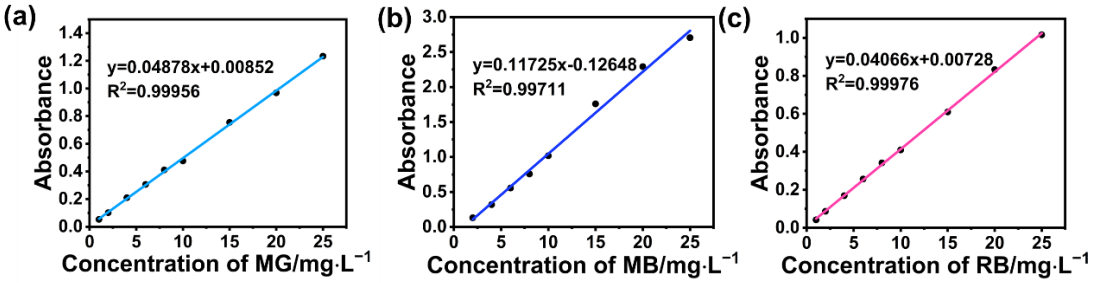

Fig. S1 The standard curves of MG, MB and RB solution.

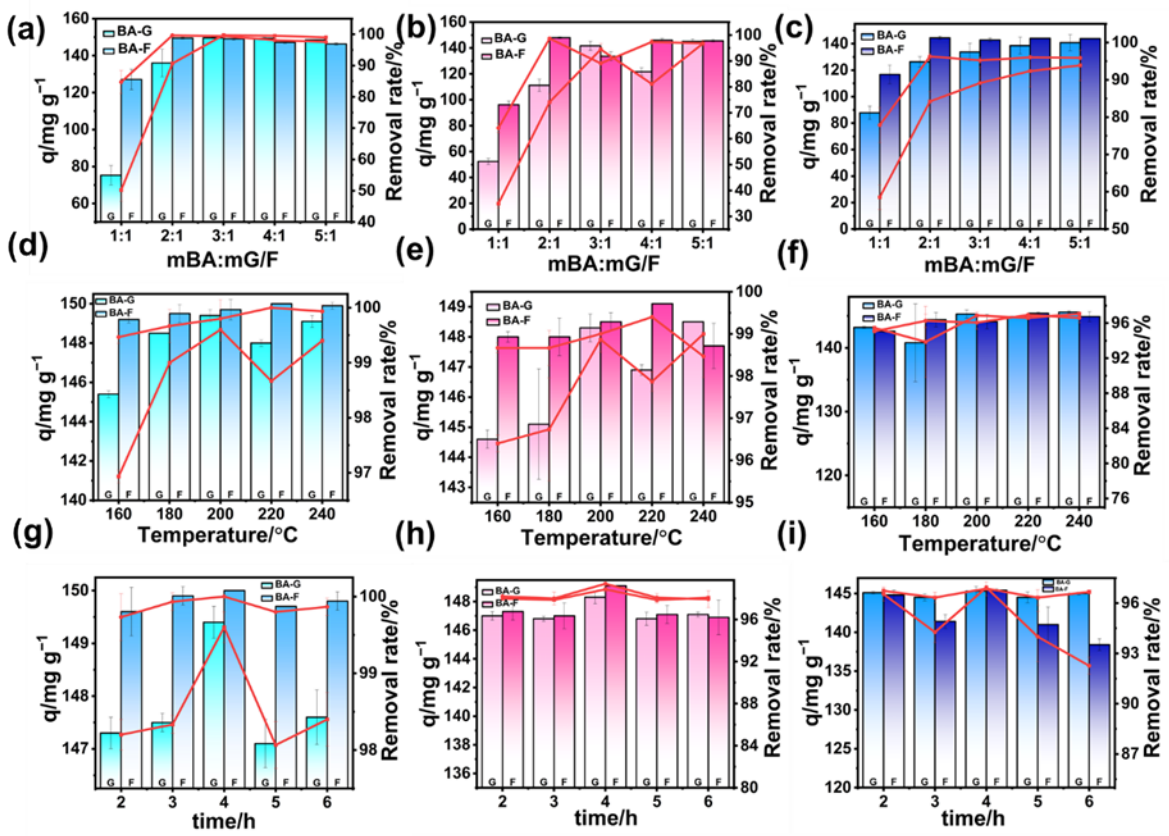

Fig. S2 Adsorption of MG, RB and MB by BA-G and BA-F under different conditions such as reaction ratios, temperatures and contact time.

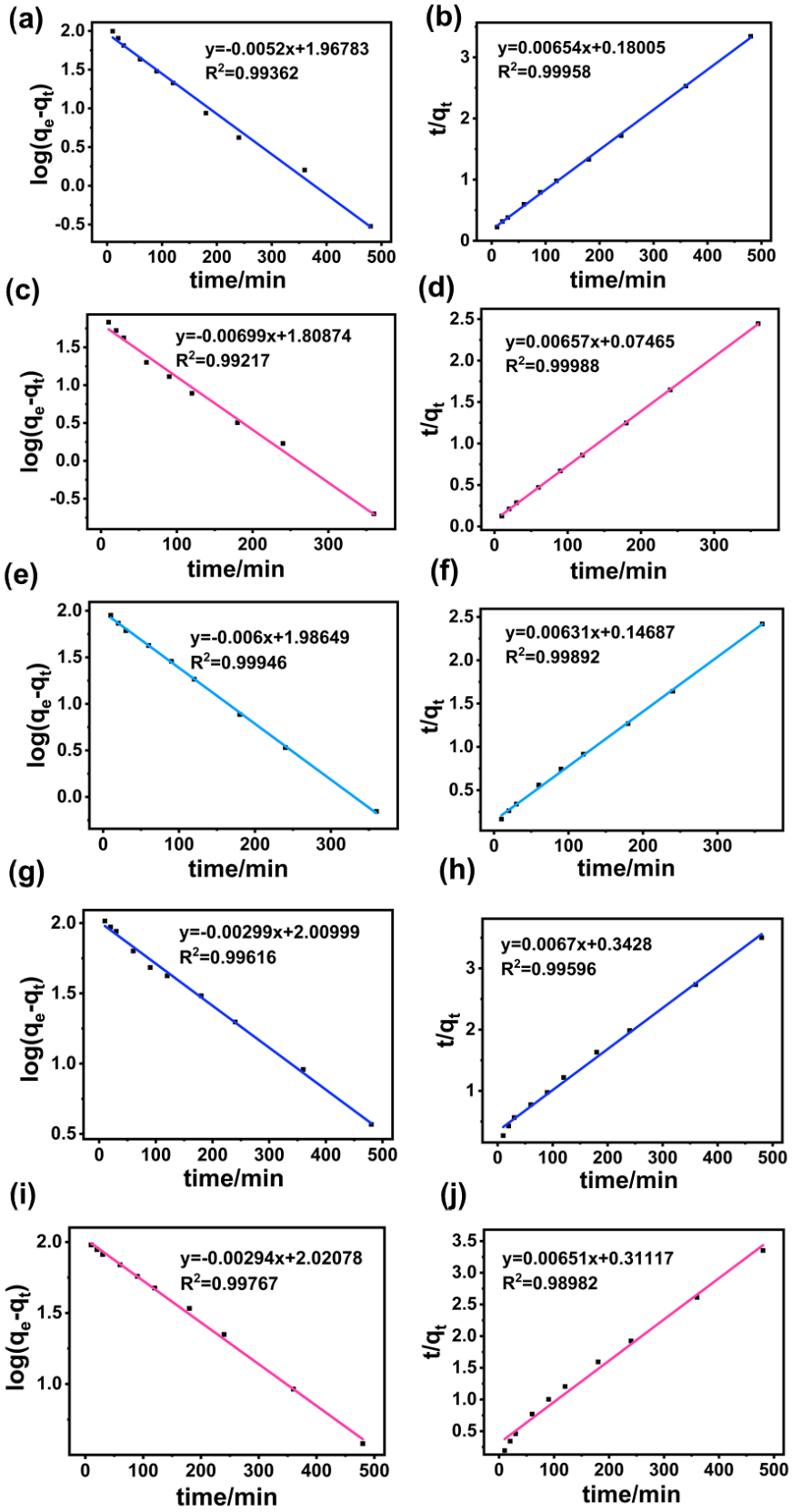

Fig. S3 Quasi-first and quasi-second order kinetic models for (a-b) BA-G-MB, (c-d) BA-G-RB, (e-f) BA-F-MG, (g-h) BA-F-MB and (i-j) BA-F-RB.

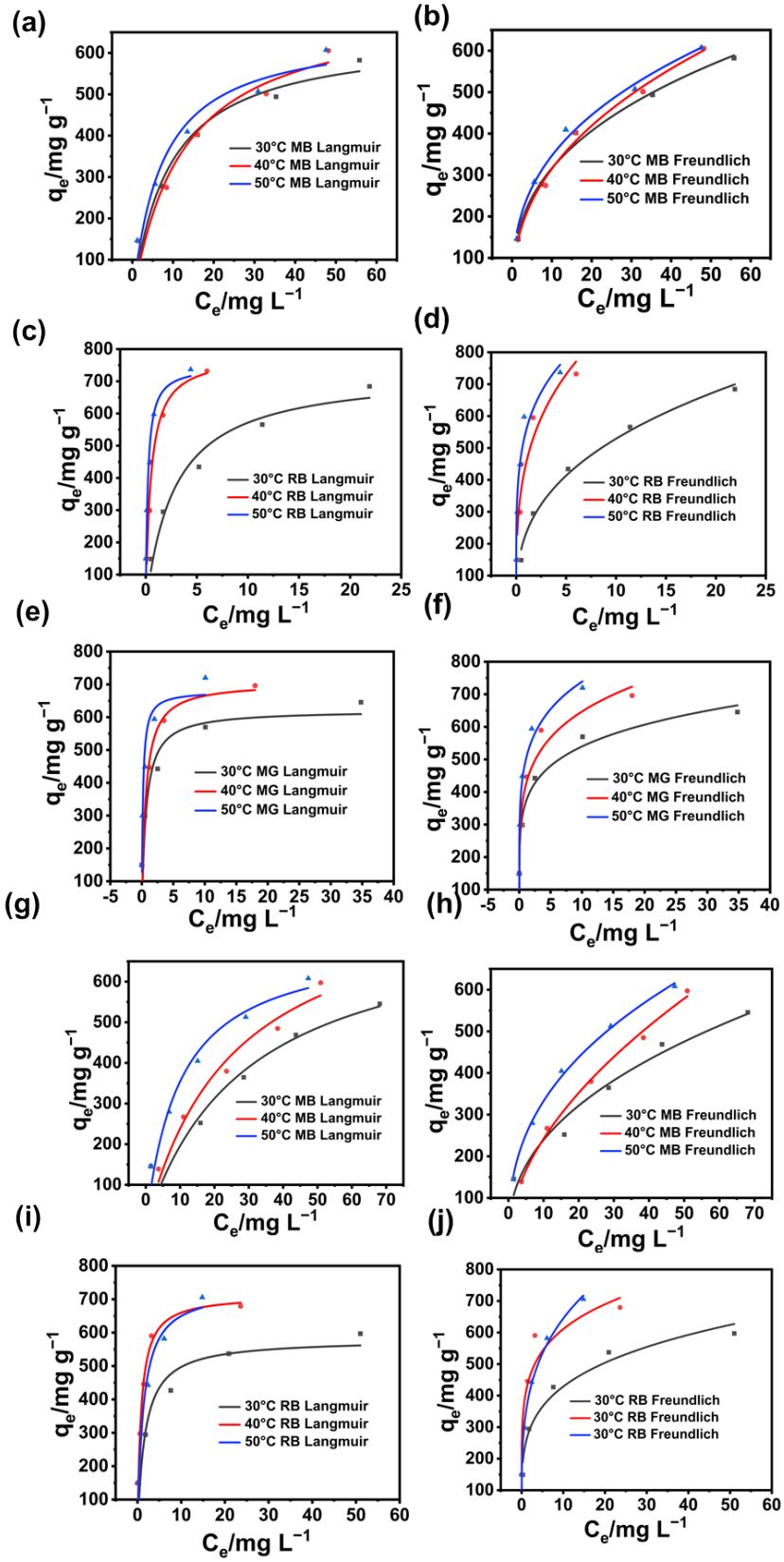

Fig. S4 Langmuir and Freundlich adsorption isotherm fitting curves for (a-b) BA-G-MB, (c-d) BA-G-RB, (e-f) BA-F-MG, (g-h) BA-F-MB and (i-j) BA-F-RB.

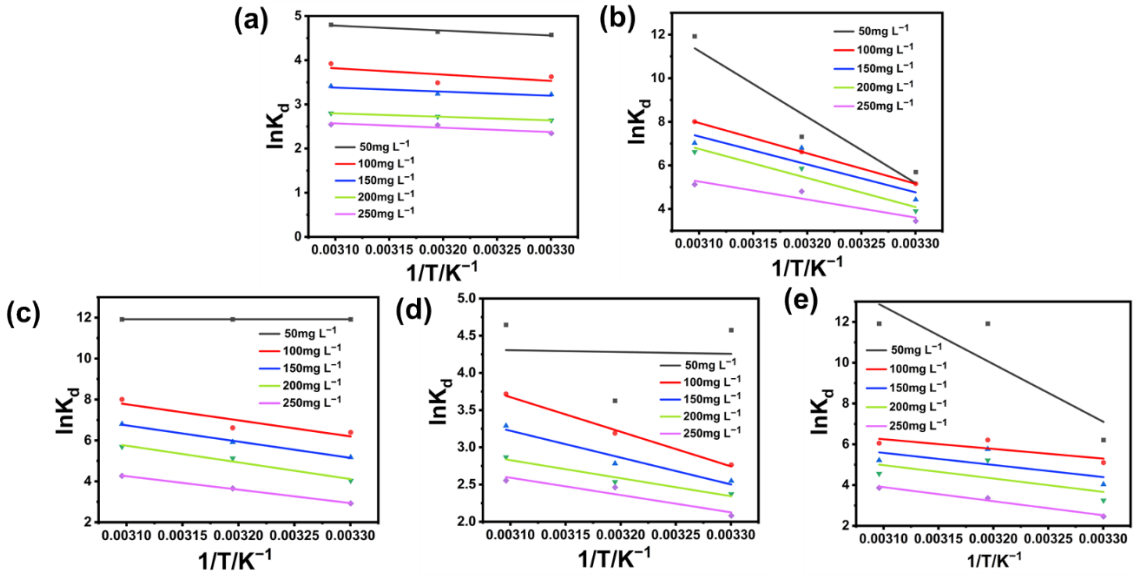

Fig. S5 Curves of lnKd vs. 1/T for (a) BA-G-MB, (b) BA-G-RB, (c) BA-F-MG, (d) BA-F-MB and (e) BA-F-RB.

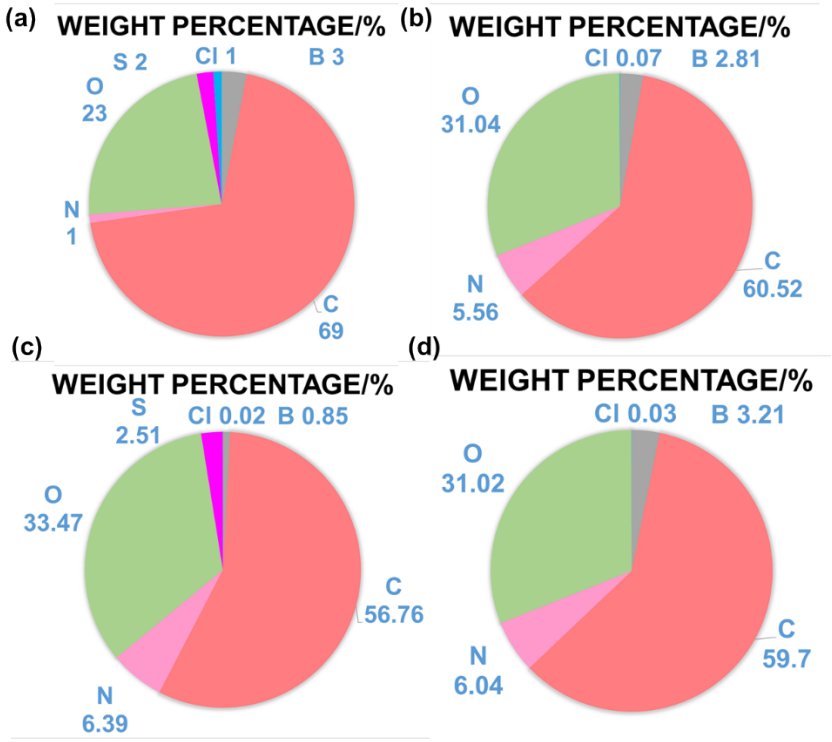

Fig. S6 EDS energy spectra of (a) BA-G-MB, (b) BA-G-RB, (c) BA-F-MB and (d) BA-F-RB.

Table S1 Parameters associated with the two kinetic models of BA-G towards

MG.

Kinetic Model	Parameters	Value
BA-G-MG-Quasi-First-Order Kinetic Model	K_1/min^{-1}	0.016
	$q_{e\ cal}$/mg g^{-1}	41.35
	R^2	0.92376
BA-G-MG-Quasi-Second-Order Kinetic Model	K_2/ g mg^{-1} min^{-1}	0.00082
	$q_{e\ cal}$/mg g^{-1}	153.14
	R^2	0.99982

Table S2 Parameters related to the two kinetic models for various types of BA-G and BA-F towards dyes.

Kinetic Model	Parameters	Value
BA-G-MB-Quasi-First-Order Kinetic Model	K_1/min^{-1}	0.012
	$q_{e\ cal}$/mg g^{-1}	92.86
	R^2	0.99362
BA-G-MB-Quasi-Second-Order Kinetic Model	K_2/ g mg^{-1} min^{-1}	0.00024
	$q_{e\ cal}$/mg g^{-1}	152.91
	R^2	0.99958
BA-G-RB-Quasi-First-Order Kinetic Model	K_1/min^{-1}	0.016
	$q_{e\ cal}$/mg g^{-1}	64.38
	R^2	0.99217
BA-G-RB-Quasi-Second-Order Kinetic Model	K_2/ g mg^{-1} min^{-1}	0.00058
	$q_{e\ cal}$/mg g^{-1}	152.21
	R^2	0.99988
BA-F-MG-Quasi-First-Order Kinetic Model	K_1/min^{-1}	0.014
	$q_{e\ cal}$/mg g^{-1}	96.94
	R^2	0.99946

BA-F-MG -Quasi-Second-Order Kinetic Model	K_2/ g mg^{-1} min^{-1}	0.00027
	$q_{e\ cal}$/mg g^{-1}	158.48
	R^2	0.99892
BA-F-MB-Quasi-First-Order Kinetic Model	K_1/min^{-1}	0.0069
	$q_{e\ cal}$/mg g^{-1}	102.33
	R^2	0.99616
BA-F-MB-Quasi-Second-Order Kinetic Model	K_2/ g mg^{-1} min^{-1}	0.00013
	$q_{e\ cal}$/mg g^{-1}	149.25
	R^2	0.99596
BA-F-RB-Quasi-First-Order Kinetic Model	K_1/min^{-1}	0.0068
	$q_{e\ cal}$/mg g^{-1}	104.90
	R^2	0.99767
BA-F-RB-Quasi-Second-Order Kinetic Model	K_2/ g mg^{-1} min^{-1}	0.00014
	$q_{e\ cal}$/mg g^{-1}	153.61
	R^2	0.98982

Table S3 Parameters related to two adsorption isotherm models of BA-G towards MG.

Temperature/℃	Langmuir			Freundlich		
	q_{max}/mg g^{-1}	K_L/L·mg^{-1}	R^2	1/n	K_F/L mg^{-1}	R^2
BA-G-30-MG	694.02	1.08	0.98807	0.24	338.78	0.90709
BA-G-40-MG	674.17	5.93	0.92385	0.15	491.07	0.84483

BA-G-50-MG	756.91	6.79	0.97217	0.17	610.90	0.48134

Table S4 Parameters related to two adsorption isotherm models for various types of BA-G and BA-F towards dyes.

Temperature /℃	Langmuir			Freundlich		
	q_{max}/mg·g^{-1}	K_L/L·mg^{-1}	R^2	1/n	K_F/L·mg^{-1}	R^2
BA-G-30-MB	644.54	0.11	0.96443	0.36	137.72	0.99146
BA-G-40-MB	723.77	0.082	0.94677	0.41	122.55	0.99205
BA-G-50-MB	657.02	0.14	0.96128	0.36	151.72	0.99283
BA-G-30-RB	732.06	0.36	0.97127	0.36	232.98	0.98948
BA-G-40-RB	784.50	2.04	0.97118	0.30	452.72	0.9042
BA-G-50-RB	748.50	5.04	0.94868	0.21	555.34	0.86412
BA-F-30-MG	621.03	1.50	0.93079	0.17	365.72	0.84681
BA-F-40-MG	706.15	1.61	0.98734	0.19	417.19	0.84517
BA-F-50-	679.64	5.73	0.9049	0.1	494.04	0.8770

MG			3	7		8
BA-F-30-MB	771.97	0.034	0.88105	0.43	89.75	0.96564
BA-F-40-MB	852.03	0.039	0.9727	0.54	69.56	0.99512
BA-F-50-MB	707.24	0.10	0.96492	0.40	133.59	0.99753
BA-F-30-RB	579.90	0.60	0.94475	0.23	250.48	0.96997
BA-F-40-RB	712.94	1.24	0.99259	0.17	408.99	0.79682
BA-F-50-RB	733.53	0.78	0.95386	0.27	344.23	0.88084

Table S5 Thermodynamic correlation parameters of BA-G towards MG.

MG concentration/mg L^{-1}	Temperature/K	ΔG^0/kJ mol^{-1}	ΔH^0/kJ mol^{-1}	ΔS^0/J mol^{-1} K^{-1}
BA-G-50-MG	303	-18.7523	217.94	781.17
	313	-26.564		
	323	-34.3758		
BA-G-100-MG	303	-13.7999	271.10	940.26
	313	-23.2025		
	323	-32.6052		
BA-G-	303	-14.393	82.38	319.39
	313	-17.5869		

150-MG	323	-20.7808		
	303	-11.6683	89.40	333.55
BA-G-	313	-15.0038		
200-MG	323	-18.3392		
	303	-8.06487	81.46	295.46
BA-G-	313	-11.0194		
250-MG	323	-13.974		

Table S6 Thermodynamic correlation parameters of BA-G and BA-F towards dyes.

The Concentration of dyes/mg L^{-1}	Temperature /K	ΔG^0/kJ mol^{-1}	ΔH^0/kJ mol^{-1}	ΔS^0/J mol^{-1} K^{-1}
	303	-11.4859	9.29	68.56
BA-G-50-MB	313	-12.1716		
	323	-12.8572		
	303	-8.89619	11.87	68.54
BA-G-100-MB	313	-9.58154		
	323	-10.2669		
	303	-8.05381	7.59	51.64
BA-G-150-MB	313	-8.57019		
	323	-9.08656		
	303	-6.64974	6.49	43.37
BA-G-200-MB	313	-7.08343		
	323	-7.51712		
	303	-5.9754	8.22	46.85
BA-G-250-MB	313	-6.44388		
	323	-6.91236		
	303	-13.0478	251.86	874.29

BA-G-50-RB	313	-21.7907		
	323	-30.5337		
	303	-12.9805	115.91	425.40
BA-G-100-RB	313	-17.2345		
	323	-21.4884		
	303	-11.9878	106.57	391.30
BA-G-150-RB	313	-15.9007		
	323	-19.8137		
	303	-10.2866	110.79	399.60
BA-G-200-RB	313	-14.2826		
	323	-18.2786		
	303	-9.07363	68.73	256.78
BA-G-250-RB	313	-11.6414		
	323	-14.2092		
	303	-25.1288	94.65	395.31
BA-F-50-MG	313	-29.0819		
	323	-33.0351		
	303	-15.6078	65.11	266.41
BA-F-100-MG	313	-18.2719		
	323	-20.936		
	303	-12.9626	65.94	260.42
BA-F-150-MG	313	-15.5668		
	323	-18.171		
	303	-10.3511	67.79	257.88
BA-F-200-MG	313	-12.9299		
	323	-15.5088		
	303	-7.38985	54.78	205.20
BA-F-250-MG	313	-9.44181		

	323	-11.4938		
	303	-10.7231	2.04	42.11
BA-F-50-MB	313	-11.1443		
	323	-11.5654		
	303	-6.90985	38.68	150.46
BA-F-100-MB	313	-8.41445		
	323	-9.91905		
	303	-6.29967	29.97	119.70
BA-F-150-MB	313	-7.49671		
	323	-8.69375		
	303	-5.90226	20.09	85.80
BA-F-200-MB	313	-6.76026		
	323	-7.61825		
	303	-5.35434	19.35	81.54
BA-F-250-MB	313	-6.16973		
	323	-6.98513		
	303	-17.8861	234.69	833.59
BA-F-50-RB	313	-26.222		
	323	-34.5579		
	303	-13.3441	39.41	174.12
BA-F-100-RB	313	-15.0853		
	323	-16.8264		
	303	-11.0609	49.33	199.30
BA-F-150-RB	313	-13.0538		
	323	-15.0468		
	303	-9.23106	54.45	210.18
BA-F-200-RB	313	-11.3328		
	323	-13.4346		

	303	-6.33951	57.29	209.99
BA-F-250-RB	313	-8.43934		
	323	-10.5392		

REFERENCES

[1] Ferreira D C M, Dos S T C, Coimbra J S D R, et al. Chitosan/carboxymethylcellulose polyelectrolyte complexes (PECs) are an effective material for dye and heavy metal adsorption from water. Carbohydrate Polymers, 2023, 315: 120977.

[2] Gao M, Xu D, Gao Y, et al. Mussel-inspired triple bionic adsorbent: Facile preparation of layered double hydroxide@polydopamine@metal-polyphenol networks and their selective adsorption of dyes in single and binary systems. Journal of Hazardous Materials, 2021, 420: 126609.

[3] Jing X R, Wang Y Y, Liu W J, et al. Enhanced adsorption performance of tetracycline in aqueous solutions by methanol-modified biochar. Chemical Engineering Journal, 2014, 248: 168-174.

[4] Zhang G, Lou X Y, Li M H, et al. A pillar[5]arene-based crosslinked polymer material for selective adsorption of organic dyes. Dyes and Pigments, 2022, 206: 110576.

[5] Qin Y, Chai B, Sun Y, et al. Amino-functionalized cellulose composite for efficient simultaneous adsorption of tetracycline and copper ions: Performance, mechanism and DFT study. Carbohydrate Polymers, 2024, 332: 121935.

[6] Kumar A S K, Warchol J, Matusik J, et al. Heavy metal and organic dye removal via a hybrid porous hexagonal boron nitride-based magnetic aerogel. npj Clean Water, 2022, 5 (1):24.

[7] Bannwarth C, Caldeweyher E, Ehlert S, et al. Extended tight-binding quantum chemistry methods. WIREs Computational Molecular Science, 2021, 11: e1493.

[8] Neese F. The ORCA program system. WIREs Computational Molecular Science, 2012, 2: 73-78.

[9] Lefebvre C, Khartabil H, Boisson J C, et al. The independent gradient model: A new approach for probing strong and weak interactions in molecules from wave function calculations. ChemPhysChem, 2018, 19, 724.
[10] Lu T, Chen F. Multiwfn: A multifunctional wavefunction analyzer. Journal of Computational Chemistry, 2012 33: 580-592.
[11] William H, Andrew D, Klaus S. VMD: Visual molecular dynamics. Journal of Molecular Graphics, 1996, 14: 33-38.